Magnetic Form Factor of Terbium*

O. STEINSVOLL,† G. SHIRANE, R. NATHANS, AND M. BLUME
Brookhaven National Laboratory, Upton, New York
AND
H. A. ALPERIN AND S. J. PICKART
U. S. Naval Ordnance Laboratory, Silver Spring, Maryland and Brookhaven National Laboratory, Upton, New York

(Received 20 March 1967)

The magnetic form factor of Tb at 4.2°K has been measured to $(\sin\theta)/\lambda=1.1$ Å^{-1} by the use of both polarized and unpolarized neutrons. The crystal was magnetized along the b and a directions by the use of a split-coil superconducting magnet providing a field of 40 kOe. At lower scattering angles where the magnetic amplitude p is greater than the nuclear amplitude b, the main source of experimental error is uncertainty in the extinction correction, which was estimated by changing wavelength as well as sample thickness. At higher scattering angles where $p<b$, the polarized-beam experiments yielded accurate form-factor values. Except for a scale factor, the measurements are in good agreement with theoretical values, suggesting a contribution from the conduction electrons which has been borne out by Fourier synthesis of the magnetization density. A theoretical calculation has been made of the aspherical contribution to the form factor.

I. INTRODUCTION

DETERMINATION of the neutron magnetic form factors of magnetic elements is of great value because their Fourier transforms give information about the spatial distribution of the magnetic-moment densities on an atomic scale. Much experimental and theoretical effort in recent years has consequently been concerned with determination of the magnetic form factors of transition-metal elements. However, while the form factors of $3d$ metals have been measured by means of polarized neutrons with considerable accuracy, no comparable measurements have been performed to date on the rare-earth metals. We have therefore carried out neutron diffraction studies of the magnetic form factor of metallic terbium, using both polarized and unpolarized neutrons.

When the investigation was initiated, the accurate measurement of anisotropic moment densities was one of the important aims, as has been the case with the similar measurements of $3d$ metals. It soon became apparent that the situation is quite different in $3d$ and $4f$ elements. In the $3d$ case, where the unpaired spins constitute the predominant part of the magnetic moment, the anisotropy of the spin density is not influenced by application of a magnetic field. The spin direction follows the magnetic field, but its spatial distribution, determined by the crystalline field, remains unchanged. On the other hand, the unquenched orbital moment in the case of rare-earth metals causes spin-orbit coupling to be larger than crystalline-field effects. Consequently, when a large enough magnetic field to align the moment is applied in a given crystallographic direction, as is required for the polarized-beam experiment, this field direction becomes the unique axis of the moment distribution. If we visualize the moment distribution as a pancake, the pancake turns with the field.

Thus the physical nature of the $4f$ moment distribution itself unfortunately deprives us of determination of the asphericity by the conventional polarized-neutron technique, since the measurement is limited to a zone of reflections with the field direction as the zone axis. We measure the projection of a pancake on its base which naturally has cylindrical symmetry. This implies, moreover, that the form-factor values measured by the polarized beam are not necessarily identical with those obtained by the unpolarized beam without magnetic field. As will be shown, the present measurements provide a reasonably accurate approximation to the spherical form factor of Tb.

Terbium crystallizes in the hcp structure with $a=3.601$ A and $c=5.694$ A at room temperature. The previous magnetic[1] and neutron[2] measurements established helical antiferromagnetism below 230°K and ferromagnetism below 220°K. From magnetization measurements at 4.2°K Hegland *et al.*[1] found a saturation moment of 9.34 μ_B along the easy b axis, and the deviation of this number from the free-ion value of 9.0 μ_B has been attributed to conduction-electron polarization. The difficulty mentioned in the previous paragraph does not of course affect the assessment of this contribution to the neutron scattering, and, as we shall see, evidence for it is provided by our measurements.

II. THEORETICAL FORM FACTOR

In order to calculate the form factor to be expected for the polarized and unpolarized-beam experiments, we start from the basic formula for the magnetic scattering cross section (as described in the Appendix)

$$(d^2\sigma/d\Omega d\epsilon)\alpha\,|\,\hat{K}\times[\mathbf{M}(\mathbf{K})\times\hat{K}]\,|^2, \qquad (1)$$

* Work performed under the auspices of the U. S. Atomic Energy Commission.
† Present address: Institutt for Atomenergi, Kjeller, Norway.

[1] D. E. Hegland, S. Legvold, and F. H. Spedding, Phys. Rev. **131**, 158 (1963).
[2] W. C. Koehler, H. R. Child, E. O. Wollan, and J. W. Cable, J. Appl. Phys. Suppl. **34**, 1335 (1963).

where K is the unit scattering vector ($=\mathbf{K}/|K|$) and $\mathbf{M}(\mathbf{K})$ is the Fourier transform of the magnetization density. The magnetic form factor $f_\eta(\mathbf{K})$ in the direction of the magnetization density

$$\hat{\eta}(\mathbf{K})=\mathbf{M}(\mathbf{K})/|\mathbf{M}(\mathbf{K})|$$

is defined by rewriting (1) as

$$|\hat{K}\times[\hat{\eta}(\mathbf{K})\times\hat{K}]|^2\,|f_\eta(\mathbf{K})|^2, \tag{2}$$

so that

$$f_\eta(\mathbf{K})=(-2mc/e\hbar)\tfrac{1}{9}|\mathbf{M}(\mathbf{K})|, \tag{3}$$

where the constants are inserted to make $f_\eta(0)=1$. As shown in the Appendix, $\mathbf{M}(\mathbf{K})$ [or its Fourier transform $\mathbf{M}(\mathbf{r})$] is the sum of spin and orbital contributions to the magnetization. Hence in order to calculate $\mathbf{M}(\mathbf{K})$ it is sufficient to calculate separately the spin and orbital contributions to the magnetization-density-operator components $M_x(\mathbf{r})$, $M_y(\mathbf{r})$, $M_z(\mathbf{r})$ and then take their Fourier transforms. For terbium we take the electronic configuration to be $(4f)^8$ so that $L=3$, $S=3$, $J=6$ and the $M=6$ level (quantized along the direction of magnetization) is assumed to be the ground state. The expectation value of the Fourier transform of the magnetization density is then calculated by using the expression of Trammel[3] for the orbital operator and the expression for the spin-magnetization-density operator given in the Appendix. Making use of the fact that the assumed ground-state wave function of Tb^{3+} is expressible as a single determinant, we find

$$M\binom{x}{y}(K)=\binom{1}{-i}\left(-\frac{e\hbar}{2mc}\right)(4\pi)^{1/2}\times\left\{-\langle g_2\rangle\frac{\sqrt{30}}{12}[Y_2^1(\hat{K})(\mp)Y_2^{-1}(\hat{K})]-\frac{3\sqrt{5}}{22}\langle g_4\rangle[Y_4^1(\hat{K})(\mp)Y_4^{-1}(\hat{K})]\right\}, \tag{4}$$

$$M_z(\mathbf{K})=\left(-\frac{e\hbar}{2mc}\right)(4\pi)^{1/2}\left\{(3\langle g_0\rangle+6\langle j_0\rangle)Y_0^0(\hat{K})-\left(\frac{\sqrt{5}}{3}\langle j_2\rangle-\sqrt{5}\langle g_2\rangle\right)Y_2^0(K)+\left(\frac{9}{11}\langle g_4\rangle-\frac{3}{11}\langle j_4\rangle\right)Y_4^0(\hat{K})\right\}, \tag{5}$$

where $Y_l^m(\theta,\phi)$ are the spherical harmonics, θ is the angle between the direction of magnetization and the scattering vector and the ϕ dependence does not appear in M_z or in the quantity of interest, $M_x^2+M_y^2$. The $\langle g_i\rangle$ and $\langle j_i\rangle$ are radial integrals which have been calculated by Blume, Freeman, and Watson[4] using Hartree-Fock wave functions.

The expressions for the form factor given here are rather complex because we have considered in detail the aspherical parts of the form factor. For the polarized-beam measurements (with an applied field in the z direction) only the component M_z is different from zero, and $\theta=90°$. Substituting this in the expressions for the spherical harmonics, we obtain for the form factor

$$f(\mathbf{K})=f_s(K)-\Delta_p, \tag{6}$$

where $f_s(K)=\frac{1}{3}\langle g_0\rangle+\frac{2}{3}\langle j_0\rangle$ is the spherical part of the form factor, and

$$\Delta_p=-0.093\langle j_2\rangle+0.034\langle j_4\rangle+0.278\langle g_2\rangle-0.102\langle g_4\rangle. \tag{7}$$

Δ_p is listed, together with f_s, in Table I. We see from these results that the aspherical contribution to the form factor is small.

The corresponding term Δ_u for the unpolarized-beam experiment is similarly complicated. Here no magnetic field is applied and the orientations of the samples are such that the c axis and the scattering vector (making an angle β with each other) were in a plane perpendicular to the a or b axes. In this case, the value of $\cos^2\theta$ is taken to be $\frac{1}{2}\sin^2\beta$, a result obtained by averaging over assumed randomly distributed ferromagnetic domains. The resulting Δ_u is given numerically in Table I, and is also seen to be relatively small.

Table II lists Δ_p, which is a unique function of $(\sin\theta)/\lambda$, for later comparison with the experimental values at higher scattering angles.

TABLE I. Theoretical form factor for Tb. The spherical part f_s is given by Eq. (6). The aspherical contribution is defined as Δ_p for polarized neutrons and Δ_u for unpolarized neutrons as explained in the text.

h	k	l	f_s	Δ_p	Δ_u
1	0	0	0.890	0.003	−0.002
0	0	2	0.873	0.003	0.003
1	0	1	0.865	0.003	0.000
1	0	2	0.785	0.006	0.002
1	0	3	0.673	0.009	0.005
2	0	0	0.660	0.010	−0.006
2	0	1	0.640	0.011	−0.004
0	0	4	0.612	0.012	0.012
2	0	3	0.517	0.015	0.003
1	0	5	0.443	0.018	0.015
3	0	0	0.428	0.018	−0.010
3	0	2	0.387	0.021	−0.006
0	0	6	0.368	0.021	0.021
1	1	0	0.722	0.008	−0.004
1	1	2	0.643	0.009	−0.001
1	1	4	0.470	0.016	0.007
2	2	0	0.340	0.022	−0.011
2	2	2	0.310	0.022	−0.008
1	1	6	0.293	0.023	0.016
2	2	4	0.243	0.025	−0.001

[3] G. T. Trammell, Phys. Rev. **92**, 1387 (1953).

[4] M. Blume, A. J. Freeman, and R. E. Watson, J. Chem. Phys. **37**, 1245 (1962); **41**, 1878 (1964).

III. EXPERIMENTAL PROBLEMS

A. Comparison of Polarized- and Unpolarized-Neutron Methods

As was mentioned in the Introduction, we have used both polarized and unpolarized neutrons for our measurements. The polarized-neutron technique yields the ratio

$$R=(b+p)^2/(b-p)^2, \quad (8)$$

where p is the magnetic and b the nuclear scattering amplitude. This method gives precise results when $p \ll b$, since the result is not sensitively dependent upon the incident polarization, spin-flipping efficiency and beam depolarization, for which R must in practice be corrected. For reflections where the value of p approaches that of b, i.e., close to the "crossover point," one has to determine these corrections with high accuracy to determine p, while at lower angles, where $p \gg b$, R becomes fairly insensitive to p. It is therefore practical to use the polarized-neutron technique for the high-angle reflections and the unpolarized technique for the low-angle reflections. In fact, we have used both methods for the whole angular region, but the data have been given preference according to their accuracy. It may be pointed out that the "crossover point" in Tb is around $(\sin\theta)/\lambda=0.55$, while in $3d$ metals this point is located at much lower angles, if it exists at all.

The integrated intensities of unpolarized neutrons are given by the familiar expression

$$I=KF^2 \exp\{-2B[(\sin\theta)/\lambda]^2\}[b^2+\langle q^2\rangle p^2], \quad (9)$$

where $\langle q^2\rangle$ depends on relative angles between the magnetic moments and the scattering vectors for a given domain distribution. Since our data were taken without magnetic field, the domain distribution must be considered as one of the experimental parameters. Another difficulty of the unpolarized-beam experiment is the accurate determination of the temperature factor B at 4°K, which was calculated from the B value determined at 300°K. Uncertainty in this process could produce an appreciable error in higher-angle reflections. A third source of error is the assumption that the scale factor K is identical at 300°K and 4°K. These uncertainties of temperature and scale factors are completely eliminated in the polarized-neutron technique, if we can assume that the temperature factor of magnetic electrons is identical to that of nuclei.

B. Extinction Effects

Secondary extinction, arising mainly from the large magnetic intensity, turned out to be the most serious source of uncertainty in our measurements. Because of the large moment of 9.34 Bohr magnetons, the scattering cross section in the ferromagnetic state increases greatly above the room-temperature value, at least for low-order reflections. This is obviously a more troublesome situation than for the $3d$ transition metals, where the atomic magnetic moments are at a maximum of the order of a few Bohr magnetons.

There are several approaches to such a problem. One is to make measurements at different neutron wavelengths and to extrapolate the data to zero wavelength, another to diminish the size of the sample and to extrapolate the data to zero dimensions. In principle, with a knowledge of the mosaic spread, it is also possible to use a theoretical extinction parameter to correct the experimental data. However, in view of the uncertainty of the latter approach, especially with relation to the polarized-neutron measurements (where peak rather than integrated intensities are measured), we decided upon a combination of the first two methods.

There is an additional internal check for extinction effects in our present experiments, namely comparison of the values obtained by polarized- and unpolarized-beam measurements. It is well known that extinction always gives a smaller diffraction cross section than the true value. For the polarized-beam technique, this results in the case of $p>b$ in a larger apparent p value, since, according to Eq. (8), R is decreasing as p increases. Since the theoretical values of form factors are quite close to each other for the two methods, as shown in Table I, the two sets of measurements thus give upper and lower limits of the true form factors for $p>b$. This criterion was effectively used to assess extinction effects in several intense low-angle lines.

TABLE II. The aspherical part of form factor Δ_p for the polarized-beam experiment. f_s is the spherical part as given by Eq. (6). It should be noted that these values are not the same as those calculated using the paramagnetic approximation [see Eq. (7) of Ref. 4].

$(\sin\theta)/\lambda$	f_s	Δ_p
0.1	0.955	0.000
0.2	0.839	0.004
0.3	0.690	0.009
0.4	0.538	0.016
0.5	0.405	0.020
0.6	0.295	0.023
0.7	0.210	0.026
0.8	0.154	0.032
0.9	0.103	0.026
1.0	0.072	0.025
1.1	0.050	0.023
1.2	0.037	0.022

IV. RESULTS

A. Unpolarized-Neutron Data

The original single crystal of terbium (dimensions $3\times3\times13$ mm^3) was cut into smaller pieces, and the measurements were performed on several small crystals with different sizes and orientations, as shown in Table III. According to the way these crystals were cut relative to the crystallographic directions they may be labeled A, B, and C crystals. The A crystal samples

TABLE III. Dimensions of Tb crystals used for the neutron diffraction experiments, in units of mm. Rotation axis corresponds to *b* and *a* axes for B- and A-type crystals, respectively.

	c axis				Rotation axis	Experiment
B1	3	×	3	×	10	Polarized
B2	1	×	1	×	10	Unpolarized
A1	3	×	3	×	3	Unpolarized
A2	0.5	×	2.0	×	1.5	Unpolarized
A3	0.9	×	1.5	×	2.5	Polarized

were mounted on the spectrometer with the *a* axis vertical to give reflections of the type (*h*0*l*), while the B and C crystals give reflections of type (*hhl*) and (*hk*0), respectively. Measurements were performed at room temperature and at liquid-helium temperature at two neutron wavelengths, $\lambda=1.05$ Å and $\lambda=0.70$ Å.

From several sets of room-temperature data the temperature factor B was determined by least squares to be $0.96\pm0.04\times10^{-16}$ cm². This value, which within our experimental limit is isotropic, corresponds to a Debye temperature of 160°K. Using this Debye temperature, one may calculate a value for B at 4.2°K of 0.115×10^{-16} cm². After subtracting the calculated nuclear contribution at 4.2°K from the total observed intensities, the remaining magnetic part was put on an absolute scale by using the nuclear scattering amplitude of $b=0.76\times10^{-12}$ cm.

The results are shown in Table IV and Fig. 1. In these, the form factors have been normalized to $p_0=2.512\times10^{-12}$ cm corresponding to 9.34 μ_B. Results which were obviously affected by extinction are not included in these tables. We believe that any extinction

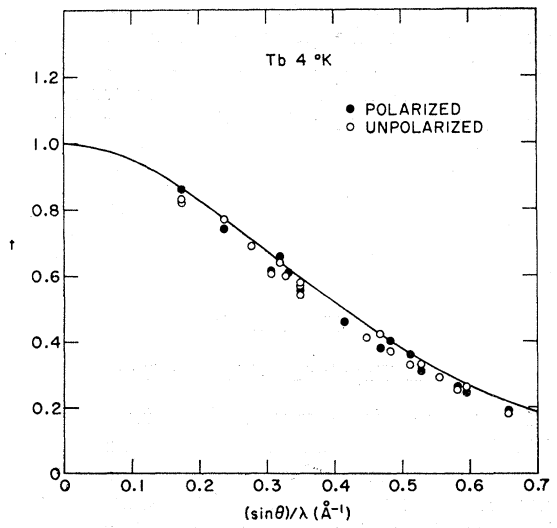

FIG. 1. Tb form-factor values at 4°K in lower-angle region from polarized- and unpolarized-neutron measurements. The smooth curve corresponds to $f_s-\Delta_p$.

effects have been experimentally reduced to the order of the discrepancies between polarized and unpolarized data at low angles. At higher angles the agreements between them are quite satisfactory.

B. Polarized-Neutron Data

In order to observe the intensity ratio for neutron spin reversal in the form given in Eq. (8), it is necessary the crystal be magnetized in a direction normal to the scattering vector. Furthermore, if the sample is not completely saturated, depolarization will occur within the crystal itself. The 40-kOe field of the superconducting magnet designed for this purpose made it possible to achieve a magnetization close to saturation in both the *a* and *b* directions of the terbium samples, resulting

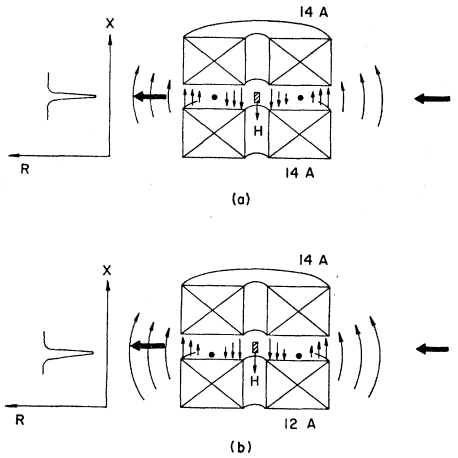

FIG. 2. Arrangement of the split-coil superconducting magnet. In (a) with the coils carrying equal current, the field-reversal region (black spot) is in the median plane. Thin arrows show the field direction along the path of the beam, indicated by the fat arrow. Plotted at the left is the polarization ratio R of an analyzing crystal as a function of height x, which indicates severe depolarization in the median plane. In (b), the coils carry unequal current and the field-reversal region moves below the median plane, where it can be avoided by the neutron beam.

in a depolarization of ~3%. To minimize the demagnetization factor, the samples were magnetized along their long dimensions, and small pieces of soft iron were fixed to both ends of the samples.

The configuration of the split-coil superconducting magnet, sketched in Fig. 2, causes additional depolarization along the path of the beam. Because of the large return field, there exists in the median plane between the coils a toroidal volume element where all magnetic field components effectively go to zero. Within this region the neutron beam is subject to severe depolarization, which could be measured by analyzing the polarization of the beam as a function of height after it had passed through the magnet [see Fig. 2(a)]. However, by adjusting the current in each coil independently and letting the lower coil carry less current than the upper this zero-field depolarizing region can be forced

to move downward out of the collimated incident neutron beam [see Fig. 2(b)]. The polarization vector of the neutron beam still has to perform an adiabatic turn with the magnetic field in the region where the vertical component changes sign, but here a horizontal component guides it across the reversal region. A polarization of 98% could be measured in the beam after it had passed through the magnet, in fact having turned twice in the process.

Two different crystal samples were used in the experiments with polarized neutrons, as shown in Table III. The measurements were performed at 4.2°K with the crystals magnetized along their long dimensions. A neutron wavelength of 0.8 Å was used which permitted measurements of the form factor up to $(\sin\theta)/\lambda \sim 1.1$ Å^{-1}.

TABLE IV. Observed low-angle magnetic-scattering amplitudes of Tb, as measured on the specified crystals. The statistical error of the measurements is less than ±0.02.

				Unpolarized		Polarized	
h	0	l	$(\sin\theta)/\lambda$	A1	A2	B2	A3
1	0	0	0.160				
0	0	2	0.175		0.83	0.82	0.86
1	0	1	0.182				
1	0	2	0.237	0.77			0.74
1	0	3	0.308	0.61			0.61
2	0	0	0.320	0.64			0.66
2	0	1	0.332				0.61
0	0	4	0.351	0.54	0.58	0.57	0.56
2	0	3	0.415				0.46
1	0	5	0.467	0.42			0.39
3	0	0	0.481	0.37			0.40
3	0	2	0.512	0.33			0.36
0	0	6	0.527	0.33	0.31	0.33	0.31
h	h	l	$(\sin\theta)/\lambda$			B2	B1
1	1	0	0.278			0.69	
1	1	2	0.328			0.60	
1	1	4	0.447			0.41	
2	2	0	0.555			0.29	
2	2	2	0.582			0.25	0.261
1	1	6	0.596			0.26	0.239
2	2	4	0.657			0.18	0.183

The small A3 sample was used to study the strong low-angle reflections, while the larger B1 sample was used for the weaker high-angle reflections, again in order to minimize secondary extinction effects. Integrated intensities obtained from the A3 crystal, when plotted against calculated intensities, showed no systematic trend indicative of secondary extinction. Since the (006) polarization ratio as measured on the B1 crystal agrees with that of the extinction-free A3 crystal, we may safely conclude that the even weaker high-angle reflections from the B1 crystal are free of extinction.

Polarization ratios were measured at the maximum of the Bragg peaks. From these data normalized form-factor values were obtained using the aforementioned values of $b=0.76\times10^{-12}$ cm for the nuclear scattering amplitude and $p_0=2.512\times10^{-12}$ cm for the forward magnetic-scattering amplitude. The effective beam polarization was taken as 93% and the spin-flipping efficiency 99%. The results are given in Tables IV and V and Figs. 1 and 3.

TABLE V. High-angle form-factor values measured by polarized neutrons on the B1 crystal.

h	h	l	$(\sin\theta)/\lambda$ (Å^{-1})	f
0	0	6	0.527	0.311±0.006
2	2	2	0.582	0.261±0.005
1	1	6	0.596	0.239±0.004
2	2	4	0.657	0.183±0.002
0	0	8	0.702	0.148±0.001
1	1	8	0.755	0.119±0.002
2	2	6	0.765	0.115±0.001
3	3	0	0.833	0.080±0.001
3	3	2	0.851	0.075±0.001
0	0	10	0.878	0.066±0.001
2	2	8	0.895	0.059±0.001
3	3	4	0.904	0.056±0.002
1	1	10	0.921	0.053±0.005
3	3	6	0.985	0.035±0.001
2	2	10	1.04	0.022±0.001
1	1	12	1.09	0.016±0.001
3	3	8	1.09	0.014±0.001
4	4	0	1.11	0.012±0.002

V. DISCUSSION

The present measurements failed to give accurate form-factor values for the two inner peaks (100) and (101), primarily due to the crystal geometry. An effort was made to overcome this problem by the measurements on a small C crystal with the dimensions of 0.4×0.4×2 mm^3. However, the distortion introduced during the cutting process made the mosaic spread of the crystal so wide that reliable values of the integrated intensities could not be obtained. In addition, powder measurements were attempted to reduce the uncertainty, but here the high room-temperature background

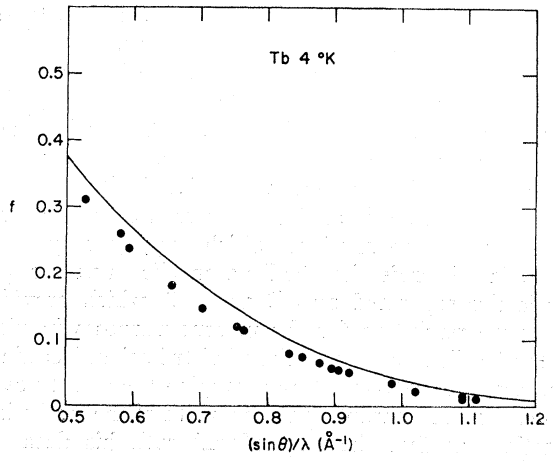

FIG. 3. Form-factor values in high-angle region, from polarized-neutron measurements only. Smooth curve as in Fig. 1.

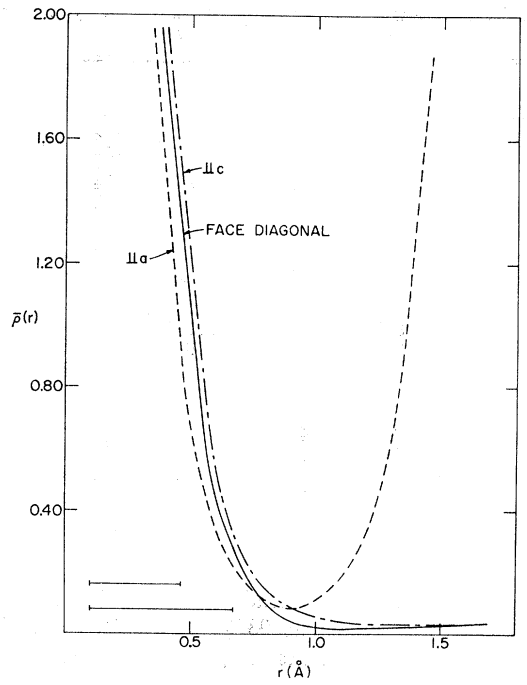

FIG. 4. Plot of the average projected magnetization density $\bar{\rho}(r)$ along several directions in the *ac* plane. The density has been averaged over a rectangle $0.1c \times 0.1a$ (the lengths shown) and is given in units of $p/\text{Å}^2$. The peak density is 5.428 or 20.178 $\mu_B/\text{Å}^2$.

from the paramagnetic scattering nullified the effort. The best estimate of these form-factor values are 0.85 ± 0.05 for (100) and 0.81 ± 0.05 for (101).

An obvious feature of Figs. 1 and 3 is that the experimental values, which were deduced by normalizing to the observed magnetization 9.34 μ_B, lie consistently lower than the theoretical values calculated on the model corresponding to 9 μ_B. One may argue that the experimental values should be scaled upward by normalizing to 9 μ_B, which is equivalent to the assumption that the remaining 0.34 μ_B is due to the polarization of the conduction electrons. In order to investigate this question independently of any assumptions about a theoretical form factor, we have synthesized the magnetization density by Fourier inversion of the measured scattering amplitudes.

Because of the large errors associated with the inner two reflections, this analysis was restricted to a projection upon the *ac* plane, which requires only (*hhl*) data. In this projection the Tb atoms lie on a rectangular lattice separated by $c/2$ and $a/2$, which provides adequate resolution for the present purposes in view of the localized nature of the 4*f* distribution. Termination errors were avoided by averaging the density over dimensions comparable with the width of the resolution function, as first done by Moon[5] with his data on hexegonal Co. In Fig. 4 we plot the density averaged over a rectangle with one-tenth the sides of the projected plane, which was determined to be sufficient to provide convergence in $(\sin\theta)/\lambda$. Along directions in which the atoms are clearly resolved, the density levels off to a residual value near 0.09 $\mu_B/\text{Å}^2$. On averaging over the area outside the localized moment and integrating over the unit cell, we arrive at a figure of 0.48 ± 0.17 μ_B/atom for this uniform polarization, where the error rises from statistical uncertainty in the scattering amplitudes.

There is a further possible source of error in the polarized-neutron measurements, namely the nuclear polarization, such as observed by Shull and Ferrier[6] in vanadium. It is impossible to calculate this effect exactly without a knowledge of the nuclear-spin scattering amplitudes of Tb, but an upper limit on their difference is set by the fact that we deduce the same p value within experimental error for cases where polarized and unpolarized measurements are of comparable accuracy. Moreover, the nuclear polarization has the effect of adding a constant to the form factor, which is opposite to the effect of a uniform polarization, which scales the form factor. In view of these considerations, we believe our analysis establishes a conduction-electron polarization at a level within the quoted error.

It may be seen, especially in Fig. 3, that the observed points lie on a smooth curve, corresponding to an isotropic moment distribution. From the Fourier projections, we find that the possible anisotropy amounts at most to 0.7% of the peak density, consistent with the cylindrical symmetry of the moment distribution discussed earlier. In over-all aspect, we may say that the agreement between the observed and calculated form factors is satisfactory.

ACKNOWLEDGMENTS

We wish to express our gratitude to Professor F. H. Spedding, Professor S. Legvold, and Dr. L. Sill of the Ames Laboratory who kindly provided the excellent terbium crystal used for the experiments. We also wish to thank Dr. W. C. Koehler, Dr. D. E. Cox, and Professor C. G. Shull for many helpful discussions.

APPENDIX

In this section a brief treatment of the orbital and spin scattering will show that this scattering can be related to the magnetization density of the scatterer. An expression for the quantum-mechanical magnetization-density operator will also be given.

The magnetic scattering cross section (assuming

[5] R. M. Moon, Phys. Rev. **136**, A195 (1964).

[6] C. G. Shull and R. P. Ferrier, Phys. Rev. Letters **10**, 295 (1963).

unpolarized neutrons) is given by[7]

$$\frac{d^2\sigma}{d\Omega d\epsilon}=\left(\frac{\gamma e^2}{mc^2}\right)^2\frac{k'}{k}\sum_{qq'}p_q\,|\,\langle q'\,|\times\sum_i e^{i\mathbf{K}\cdot\mathbf{r}_i}\left(\hat{K}\times(\mathbf{s}_i\times\hat{K})-\frac{i}{K}\hat{K}\times\mathbf{p}_i\right)|\,q\rangle\,|^2\times\delta\left(\frac{\hbar^2}{2m_0}(k'^2-k^2)+E_{q'}-E_q\right).\tag{A1}$$

Notation: $\gamma=-1.91$ is the gyromagnetic ratio of the neutron; $|\,q\rangle$ and $|\,q'\rangle$ are the initial and final states of the scatter with energies E_q and $E_{q'}$; p_q is the probability that $|\,q\rangle$ is occupied; $\mathbf{r}_i$, $\mathbf{p}_i=-\nabla_i$, s_i are the position, momentum, and spin operators of the ith electron of the scatter (the latter two in units of $\hbar$); m and m_0 are the electron and neutron masses; the scattering vector $\mathbf{K}=\mathbf{k}_i-\mathbf{k}_f$, where $\mathbf{k}_i$ and $\mathbf{k}_f$ are the initial and final neutron wave vectors; and the remaining notation has been defined in the text. We will consider the operator in the matrix element of (A1). The term $\sum_i e^{i\mathbf{K}\cdot\mathbf{r}_i}\hat{K}\times(\mathbf{s}_i\times\hat{K})$ gives the spin scattering, and $-(i/K)\sum_i e^{i\mathbf{K}\cdot\mathbf{r}_i}(\hat{K}\times\mathbf{p}_i)$ gives the orbital scattering. The spin term can be rewritten by using the transformation

$$\sum_i e^{i\mathbf{K}\cdot\mathbf{r}_i}\mathbf{s}_i=\int d\mathbf{r}\,e^{i\mathbf{K}\cdot\mathbf{r}}\sum_i\mathbf{s}_i\delta(\mathbf{r}-\mathbf{r}_i)=-\frac{mc}{e\hbar}\int dr\,e^{i\mathbf{K}\cdot\mathbf{r}}\mathbf{M}^s(\mathbf{r}),$$

where

$$\mathbf{M}^s(\mathbf{r})=-\frac{e\hbar}{mc}\sum_i\mathbf{s}_i\delta(\mathbf{r}-\mathbf{r}_i)\tag{A2}$$

is (to within the gradient of a scalar quantity) the spin-magnetization-density operator. The orbital part of the scattering has, as written in (A1), a somewhat different appearance from the spin term. In the following it is shown that the orbital terms can be transformed to give an expression analogous to (A2).

Consider

$$-\frac{i}{K}\sum_i e^{i\mathbf{K}\cdot\mathbf{r}_i}(\hat{K}\times\mathbf{p}_i)=-\frac{i}{2K}\times\sum_i[e^{i\mathbf{K}\cdot\mathbf{r}_i}(\hat{K}\times\mathbf{p}_i)+(\hat{K}\times\mathbf{p}_i)e^{i\mathbf{K}\cdot\mathbf{r}_i}]\tag{A3}$$

($\hat{K}\times\mathbf{p}_i$ commutes with $\mathbf{K}\cdot\mathbf{r}_i$). We can write

$$\tfrac{1}{2}\sum_i(e^{i\mathbf{K}\cdot\mathbf{r}_i}\mathbf{p}_i+\mathbf{p}_i e^{i\mathbf{K}\cdot\mathbf{r}_i})=\tfrac{1}{2}\int e^{i\mathbf{K}\cdot\mathbf{r}}\sum_i[\mathbf{p}_i\delta(\mathbf{r}-\mathbf{r}_i)+\delta(\mathbf{r}-\mathbf{r}_i)\mathbf{p}_i]d\mathbf{r}=-\frac{m}{e\hbar}\int e^{i\mathbf{K}\cdot\mathbf{r}}\mathbf{j}(\mathbf{r})\,d\mathbf{r},\tag{A4}$$

[7] M. Blume, Phys. Rev. **130**, 1670 (1963).

where

$$\mathbf{j}(\mathbf{r})=-\frac{e\hbar}{2m}\sum_i[\mathbf{p}_i\delta(\mathbf{r}-\mathbf{r}_i)+\delta(\mathbf{r}-\mathbf{r}_i)\mathbf{p}_i]$$

is the electronic orbital current-density operator. This can be expressed as the sum of the curl of a vector and the gradient of a scalar:

$$\mathbf{j}(\mathbf{r})=c\nabla\times\mathbf{M}^L(\mathbf{r})+\nabla\phi(\mathbf{r}).\tag{A5}$$

$\mathbf{M}^L(\mathbf{r})$ can be identified as the orbital-magnetization-density operator. (The term $\nabla\phi$ is the "longitudinal" or "conduction" current, and $c\nabla\times\mathbf{M}^L$ is the "transverse" or "molecular" current.) Substituting (A5) in (A4), integrating by parts, and discarding surface terms gives

$$\int e^{i\mathbf{K}\cdot\mathbf{r}}\mathbf{j}(\mathbf{r})\,d\mathbf{r}=-ic\mathbf{K}\times\int e^{i\mathbf{K}\cdot\mathbf{r}}\mathbf{M}^L(\mathbf{r})\,d\mathbf{r}-i\mathbf{K}\int e^{i\mathbf{K}\cdot\mathbf{r}}\phi(\mathbf{r})\,d\mathbf{r},$$

and using this in (A3),

$$-\frac{i}{K}\sum_i e^{i\mathbf{K}\cdot\mathbf{r}_i}(\hat{K}\times\mathbf{p}_i)=-\frac{mc}{e\hbar}\int e^{i\mathbf{K}\cdot\mathbf{r}}\hat{K}\times(\mathbf{M}^L(\mathbf{r})\times\hat{K})\,d\mathbf{r},$$

which has the same form as the spin scattering operator. (Note that the "longitudinal" current has dropped out, so that it makes no contribution to the neutron scattering.) We may combine these results to give

$$\sum_i e^{i\mathbf{K}\cdot\mathbf{r}_i}\left\{\hat{K}\times(\mathbf{s}_i\times\hat{K})-\frac{i}{K}\hat{K}\times\mathbf{p}_i\right\}=-\frac{mc}{e\hbar}\int e^{i\mathbf{K}\cdot\mathbf{r}}\hat{K}\times[\mathbf{M}(\mathbf{r})\times\hat{K}]d\mathbf{r}=-\frac{mc}{e\hbar}\hat{K}\times[\mathbf{M}(\mathbf{K})\times\hat{K}],\tag{A6}$$

with

$$\mathbf{M}(\mathbf{r})=\mathbf{M}^L(\mathbf{r})+\mathbf{M}^s(\mathbf{r}),\quad\text{and}\quad\mathbf{M}(\mathbf{K})=\int e^{i\mathbf{K}\cdot\mathbf{r}}\mathbf{M}(\mathbf{r})\,d\mathbf{r}.$$

An explicit expression for $\mathbf{M}^L(\mathbf{r})$ can be obtained from (A5) together with the condition,[8] $\nabla\cdot\mathbf{M}^L(\mathbf{r})=(1/2c)\nabla\cdot[\mathbf{r}\times\mathbf{j}(\mathbf{r})]$. Using the vector identity[9]

$$\mathbf{M}(\mathbf{r})=\frac{1}{4\pi}\nabla\times\int\frac{\nabla'\times\mathbf{M}(\mathbf{r}')}{|\,\mathbf{r}-\mathbf{r}'\,|}d\mathbf{r}'-\frac{1}{4\pi}\nabla\int\frac{\nabla'\cdot\mathbf{M}(\mathbf{r}')}{|\,\mathbf{r}-\mathbf{r}'\,|}d\mathbf{r}',$$

[8] L. I. Landau and E. M. Lifshitz, *Electrodynamics of Continuous Media* (Pergamon Press, Ltd., London, 1960).

[9] W. K. H. Panofsky and M. Phillips, *Classical Electricity and Magnetism* (Addison-Wesley Publishing Company, Inc., Reading, Massachusetts, 1955).

we have

$$\mathbf{M}^L(\mathbf{r}) = \frac{1}{4\pi c}\nabla\times\int\frac{\mathbf{j}(\mathbf{r}')}{|\mathbf{r}-\mathbf{r}'|}d\mathbf{r}' - \frac{1}{8\pi c}\nabla\nabla\cdot\int\frac{\mathbf{r}'\times\mathbf{j}(\mathbf{r}')}{|\mathbf{r}-\mathbf{r}'|}d\mathbf{r}', \quad \text{(A7)}$$

which, together with (A2), defines the magnetization-density operator. This expression together with the transformation of $\mathbf{j}(\mathbf{r})$ introduced by Trammell[3] gives an expression which is useful for calculations of magnetization densities in ions, where angular momentum is conserved. (A7) can be used directly to calculate orbital-magnetization densities in metals, where the electrons are described by Bloch waves. On introducing these transformations in (A1), that equation becomes

$$\frac{d^2\sigma}{d\Omega d\epsilon} = \left(\frac{\gamma e}{\hbar c}\right)^2\frac{k'}{k}\sum_{qq'}p_q|\langle q'|\hat{K}\times[\mathbf{M}(\mathbf{K})\times\hat{K}]|q\rangle|^2 \times\delta\left(\frac{\hbar^2}{2m_0}(k'^2-k^2)+E_{q'}-E_q\right).$$

Note that only the transverse-magnetization density $\hat{K}\times[\mathbf{M}(\mathbf{K})\times\hat{K}]=\mathbf{M}(\mathbf{K})-K[K\cdot\mathbf{M}(\mathbf{K})]$ contributes to the neutron scattering.

PHYSICAL REVIEW VOLUME 161, NUMBER 2 10 SEPTEMBER 1967

Statistical Mechanics and Origin of the Magnetoelectric Effect in Cr_2O_3*

R. HORNREICH† AND S. SHTRIKMAN

Department of Electronics, The Weizmann Institute of Science, Rehovoth, Israel

(Received 16 January 1967; revised manuscript received 14 April 1967)

Expressions for the temperature dependence of the magnetoelectric susceptibility parallel and perpendicular to the trigonal axis in Cr_2O_3 are presented. A two-sublattice model is used. The relation between the sublattice magnetization and the temperature is derived from experimental results for the parallel magnetic susceptibility. All statistical averages appearing in the expressions for the magnetoelectric susceptibilities are then evaluated using this susceptibility-derived result. Using this technique, quantitative agreement with the experimental results is obtained. For the parallel case, three mechanisms that have been previously proposed as contributing to the parallel magnetoelectric susceptibility are considered. It is concluded that the parallel effect is dominated at low temperatures by the electric-field-induced g shift and at higher temperatures by the electric-field-induced shift in the intrasublattice exchange energy. For the perpendicular case, three mechanisms are also considered; two of them, an electric-field-induced antisymmetric exchange term and an electric-field-induced g shift, have not previously been discussed. It is concluded that the perpendicular effect is dominated by the electric-field-induced shift in the single-ion anisotropy energy. Crystal-field aspects of the perpendicular effect are presented, and it is argued that the electric-field-induced g shift is actually 1–2 orders of magnitude smaller than the crystal-field estimate.

INTRODUCTION

THE possibility of a linear magnetoelectric (ME) effect, wherein a material exhibits an induced magnetization which is proportional to an applied electric field and an induced electric moment which is proportional to an applied magnetic field, was first pointed out by Landau and Lifshitz.[1] Such an effect can exist only in materials having an ordered magnetic structure. Dzyaloshinski[2] subsequently pointed out that the ME effect should exist in Cr_2O_3, and the electrically induced effect was first observed in this material by Astrov.[3] This was followed by the observation of the magnetically induced ME effect in Cr_2O_3 by Rado and Folen.[4] Further work[5–7] showed that the ME effect in Cr_2O_3 is strongly anisotropic and temperature-dependent.

The first proposal of an atomic mechanism that could provide an explanation of the ME effect was made by Rado.[8] He indicated that the dependence of the single-ion anisotropy energy on an externally applied field would cause an ME effect both parallel and

* Research sponsored in part by the U. S. Air Force Materials Laboratory Research and Technology Division AFSC through the European Office of Aerospace Research, U. S. Air Force Contract No. AF 61(052)-654 and was done in partial fulfillment of the Ph.D. requirements of one of the authors (R. M. H.).

† Present address: Applied Research Laboratory, Sylvania Electronic Systems, Waltham, Massachusetts.

[1] L. D. Landau and E. M. Lifshitz, *Electrodynamics of Continuous Media* (Addison-Wesley Publishing Company, Inc., Reading, Massachusetts, 1960), p. 119.

[2] I. E. Dzyaloshinski, Zh. Eksperim. i Teor. Fiz. **37**, 881 (1959) [English transl.: Soviet Phys.—JETP **10**, 628 (1960)].

[3] D. N. Astrov, Zh. Eksperim. i Teor. Fiz. **38**, 984 (1960) [English transl.: Soviet Phys.—JETP **11**, 708 (1960)].

[4] G. T. Rado and V. J. Folen, Phys. Rev. Letters **7**, 310 (1961).

[5] D. N. Astrov, Zh. Eksperim. i Teor. Fiz. **40**, 1035 (1961) [English transl.: Soviet Phys.—JETP **13**, 729 (1961)].

[6] V. J. Folen, G. T. Rado, and E. W. Stalder, Phys. Rev. Letters **6**, 607 (1961).

[7] S. Shtrikman and D. Treves, Phys. Rev. **130**, 986 (1963).

[8] G. T. Rado, Phys. Rev. Letters **6**, 609 (1961).